crystals

MDPI

Article

Crystallographic Studies on Non-Covalent Interactions in Aryl-Substituted Antimony Organometallics

Ana Torvisco *,†, Melanie Wolf †, Roland C. Fischer and Frank Uhlig

Institute of Inorganic Chemistry, Graz University of Technology, Stremayrgasse 9/V, 8010 Graz, Austria; roland.fischer@tugraz.at (R.C.F.)

* Correspondence: ana.torviscogomez@tugraz.at

† These authors contributed equally to this work.

Abstract: A series of novel and previously published organoantimony compounds (R_nSbX_{3-n}, X = Cl, Br; R = *o*-tolyl, 2,6-xylyl, 1-naphthyl, and 9-anthracenyl), were synthesized and characterized. In addition, single-crystal X-ray diffraction was employed to elucidate the molecular structures of all solid species. These compounds display non-covalent intermolecular interactions in the form of edge-to-face, π···π stacking, and CH_3···π interactions, and the effects of the substituent type and substituent bulk on the nature of these interactions present will be highlighted and discussed.

Keywords: organoantimony; solid-state structures; intermolecular interactions

check for updates

Citation: Torvisco, A.; Wolf, M.; Fischer, R.C.; Uhlig, F. Crystallographic Studies on Non-Covalent Interactions in Aryl-Substituted Antimony Organometallics. *Crystals* **2024**, *14*, 860. https://doi.org/10.3390/cryst14100860

Academic Editor: Elizabeth A. Hillard

Received: 13 September 2024
Revised: 26 September 2024
Accepted: 28 September 2024
Published: 29 September 2024

1. Introduction

While the field of organoantimony chemistry afforded early interest after the preparation of the first organoantimony compound around 1850, it has been neglected within the last years [1]. To date, aryl-substituted antimony compounds have shown feasible application in organic synthesis, coordination chemistry, or as precursors for other organometallic compounds. Synthetic applications of organoantimony compounds are rapidly increasing, with a wide variety of possible reactions and applications known, including self-coupling reactions, photoreactions, and cross-coupling as well as employment in photochemical and electrochemical devices and as precursors in solar cells, battery materials, or nanoparticles [2–13].

Tervalent stibanes have been investigated to a lesser extent than the pentavalent organic compounds of antimony [6,14]. The most common methods to prepare tervalent organometallic antimony compounds include the employment of Grignard or organometallic reagents, in the latter case, e.g., organolithium, organomercury, or organocadmium, although this highly depends on the ligands used [15–18]. These preparations are often accompanied with difficulties in reaction control, workup, and low yields [19]. In the case of organoantimony halides thermolysis of the corresponding pentacoordinate species R_3SbX_2 with loss of an alkyl or aryl halide, arylation using group 14 element compounds or comproportionation reactions between R_3Sb with SbX_3 have been employed [9,19–24]. The number of known compounds decreases dramatically if compounds bearing an element–element bond are considered, with the first ones being prepared in the 1980s. Compounds containing Sb-b bonds have gained interest due to their unusual color phenomena and possible application as ligands [16,25–28].

Of specific interest would be arylantimony(III) hydrides (R_nSbH_{3-n}), which can be readily prepared from the halide species (R_nSbX_{3-n}, X = Cl, Br) discussed in this publication via reducing the formed halides with $LiAlH_4$ to the corresponding hydrides [29–34]. These have been limited to species coordinated to 2,4,6-mesityl [35] and the larger and more sterically hindering aryl residues terphenyl [31–34] and Fluind [36,37] substituents. While these sterically hindering aryl residues result in relatively stable antimony hydride species, smaller and more volatile aryl residues would be beneficial for use of arylantimony(III)

hydrides as precursors or as dopants in semiconductors via chemical vapor deposition [30]. Moreover, as was observed for group 14 metal hydrides [38,39], arylantimony hydrides would be an interesting starting point towards antimony-based nanomaterials via dehydrocoupling reactions [40–42].

As an entry point towards arylantimony(III) hydrides, a range of known and previously unknown homoleptic, non-functionalized aryl-substituted antimony tervalent species (R_3Sb, R = 2,6-xylyl (**1**), 1-naphthyl (**2a** and **2b**), monobromides (R_2SbBr, R = 2,6-xylyl (**3**), 9-anthracenyl (**5**)), dichloride ($RSbCl_2$, R = *o*-tolyl (**4**), and a diaryldistibane ($[R_2Sb]_2$, R = 9-anthracenyl (**6**)) have been synthesized and investigated. The solid-state structures of the presented compounds display intermolecular interactions and are highlighted and discussed.

2. Results and Discussion

2.1. Synthesis

While compounds 2,6-xylyl$_3$Sb (**1**), 1-naphthyl$_3$Sb (**2**), 2,6-xylyl$_2$SbBr (**3**), as well as o-tolylSbCl$_2$ (**4**) have been characterized and reported, to our knowledge, the crystal structures of compounds **2**–**4** have not been reported [43–46]. Compounds 9-anthracenyl$_2$SbBr (**5**) and [9-anthracenyl$_2$Sb]$_2$ (**6**) bearing the 9-anthracenyl moieties are, to the best of our knowledge, the first Sb anthracene compounds to be prepared and fully characterized. The compounds 2,6-xylyl$_3$Sb (**1**), 1-naphthyl$_3$Sb (**2**), 2,6-xylyl$_2$SbBr (**3**), and anthracenyl$_2$SbBr (**5**) were synthesized using the Grignard route (Figure 1).

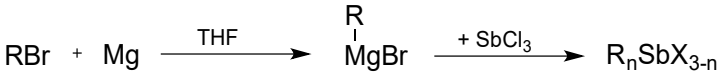

Figure 1. Grignard reaction for the preparation of organoantimony compounds with R = o-tolyl, 2,6-xylyl (**1**,**3**), 1-naphthyl (**2**), and 9-anthracenyl (**5**).

In a typical reaction, a flask equipped with a dropping funnel and a reflux condenser was charged with Mg in THF. The dropping funnel was charged with arylbromide in THF, about 10% of the solution was added to the reaction vessel, and the solution was heated carefully to start the reaction. The arylbromide was subsequently added slowly. After complete addition, the reaction was refluxed overnight. A second flask equipped with a mechanical stirrer and a reflux condenser was charged with $SbCl_3$ in THF and cooled to 0 °C. The Grignard solution was added to the $SbCl_3$ solution using a cannula and stirred overnight at room temperature. After removal of THF, toluene was added to facilitate salt elimination, and the mixture was filtered using a cannula. All solvents were evaporated under reduced pressure to obtain the desired products. All products were usually purified via recrystallization at low temperatures or via evaporation. All of the compounds obtained were stable at room temperature and showed no distinctive reactivity towards decomposition when in contact with air.

The interaction between the aryl Grignard reagent and $SbCl_3$ was, in some cases, accompanied by the precipitation of finely dispersed antimony. If stoichiometry was not applied correctly, mixtures of both 2,6-xylyl$_3$Sb (**1**) and 2,6-xylyl$_2$SbBr (**3**) were observed, making purification difficult due to similar physical properties. When exactly three equivalents of RMgBr towards $SbCl_3$ were employed, 2,6-xylyl$_2$SbBr (**3**) was formed directly without any byproducts, yielding the bromine derivative due to halide exchange. In all other cases, 2,6-xylyl$_3$Sb (**1**) was obtained as the main product.

The sterically less demanding ligands 1-naphthyl and *o*-tolyl lead to the formation of 1-naphthyl$_3$Sb (**2**) or *o*-tolyl$_3$Sb [43], respectively. This leads to the conclusion that the structure and physical/chemical properties of aryl-substituted antimony compounds depend, to a great extent, on the ligands or, more specifically, on the substituents of the phenyl ring used, which has been described previously [19,47]. Yields were generally better for *o*-tolyl and 1-naphthyl than for the 2,6-xylyl derivatives. The yields of 1-naphthyl$_3$Sb (**2**) varied due to difficulties in handling. 1-naphthylMgBr tends to crystallize upon cooling

to room temperature. This can be avoided by either using larger amounts of solvent or by cannulation whilst still hot.

The level of difficulty concerning synthesis is increased when employing the 9-anthracenyl moiety. In these cases, the Grignard reaction was difficult to start, which could be enhanced using 2-bromoethane and heat, but the yields remained generally low. Additionally, free anthracene was formed during the course of the reaction, not only lowering the yields but also overcomplicating the workup procedures, as has been reported for the silicon derivatives [48]. While the same procedure was carried out substituting $SbCl_3$ with $SbBr_3$, the distibane [9-anthracenyl$_2$Sb]$_2$ (**6**) was obtained, and after recrystallization from toluene and pentane, orange crystals were obtained. The formation of [9-anthracenyl$_2$Sb]$_2$ (**6**) is presumably the result of incomplete conversion of the Grignard reagent, since the formation of distibanes upon reaction with metals has been reported [19].

o-tolylSbCl$_2$ (**4**) was prepared via a redistribution reaction between *o*-tolyl$_3$Sb, which was prepared according to the literature, and $SbCl_3$ in a 1:2 ratio (Figure 2) [43]. Since redistribution reactions performed neat generally resulted in a mixture of products, the reactions were carried out in Et_2O analogously to the preparation of phenyl derivatives [19,24,49].

Figure 2. Preparation of *o*-tolylSbCl$_2$ (**4**) via redistribution reactions.

$SbCl_3$ was dissolved in dry Et_2O and added dropwise to a solution of *o*-tolyl$_3$Sb in dry Et_2O. The reaction was refluxed for 4 h and afterwards stirred at room temperature overnight. After removal of solvent under vacuo, the colorless solid was recrystallized. Recrystallization was best achieved when the product was dissolved in toluene and layered with a few drops of heptane [43]. 2,6-xylyl$_2$SbBr (**3**) was prepared not only by the employment of a Grignard reagent but also via the reaction between 2,6-xylyl$_3$Sb (**1**) and $SbBr_3$ in a 2:1 ratio in the same manner as *o*-tolylSbCl$_2$ (**4**) (Figure 3). In this case, $SbBr_3$ was employed for comparison with the compound prepared using the Grignard route.

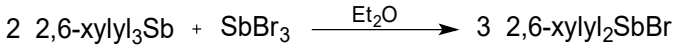

Figure 3. Preparation of 2,6-xylyl3Sb (**1**) via redistribution reactions.

2.2. X-ray Crystallography

A large variety of aromatic antimony compounds display stabilizing forces originating from the substituent on the metal center. Specifically, secondary non-covalent interactions are electrostatic interactions in the form of π-stacking stemming from the aromatic substituents [50–54] and van der Waals contacts from the halogenide substituent and adjacent hydrogens, C–H···X (X = Cl, Br) [55–60]. While individually these are weak interactions, combined they offer an overall stabilizing effect to these molecules in the solid state and aid in their crystallization. The role of aromatic non-covalent interactions in the stabilization of compounds in the solid state and their importance in chemical and biological processes have been well documented [50–54]. However, their presence and, ultimately, their effect on arylstibane species have been rarely discussed or simply overlooked. Additionally, the Lewis acidic nature of the antimony metal center varies with the nature of the substituent, and, consequently, further secondary interactions (Sb···C(π), Sb···X) [49,61,62] can arise in the solid state to afford stabilization.

In an effort to expand the existing library of compounds and study the underlying factors leading to solid-state structures, we compare a series of known and novel arylstibane compounds with aryl substituents ranging in steric demand from phenyl to polyaromatic substituents, such as 9-anthracenyl. The types of non-covalent interactions present in these systems will be highlighted and compared to previously reported compounds. In addition, the nature of the aromatic substituent and its direct effects on the type of electrostatic interaction that arises in these structures will be discussed.

2.2.1. Triaryl Stibanes or R_3Sb

The compounds 2,6-xylyl$_3$Sb (**1**), 1-naphthyl$_3$Sb·toluene (**2a**), and 1-naphthyl$_3$Sb·benzene (**2b**) are comparable to previously reported homoleptic, non-functionalized triarylstibanes (Table 1). Each molecule is in a near trigonal pyramidal geometry with the Sb atom above the plane of the rings. With respect to averaged Sb–C bond lengths, these are affected by the degree of bulkiness afforded by the organic substituent onto the antimony atom. In phenyl$_3$Sb [63–69], an averaged Sb–C bond length of 2.148(8) Å is observed. Steric bulk is not dependent on the addition of methyl substituents to the aryl residue but rather on its relative position on the aromatic ring. Therefore, the addition of a methyl group in *p*-tolyl$_3$Sb [70] results in a similar bond length of 2.141 Å to that of 2.148(8) Å in phenyl$_3$Sb [63–69]. The steric bulk effect on the Sb–C bond length becomes more apparent as the methyl substituent is at the *ortho* position, as observed in *o*-tolyl$_3$Sb [71] (2.164(6) Å). The fused aromatic residues in 1-naphthyl$_3$Sb·toluene (**2a**), 1-naphthyl$_3$Sb·benzene (**2b**), and 9-phenanthrenyl$_3$Sb [72] seem to offer a similar steric bulk as *o*-tolyl$_3$Sb [71], with averaged Sb–C bond lengths of 2.162(3) Å, 2.162(2) Å, and 2.157(4) Å, respectively. However, the effects of the steric bulk on the Sb–C bond is most pronounced when the aryl residue is substituted at both the 2- and 6-positions, as observed for the methyl substituted 2,6-xylyl$_3$Sb (**1**) [45] (2.190(2) Å), 2,4,6-mesityl$_3$Sb [73] (2.184(8) Å), and the *iso*-propyl substituted (2,4,6-^{i}propyl$_3$-C$_6$H$_2$)$_3$Sb [74] (2.184(8) Å). These display the longest Sb–C bond lengths. In conjunction with the increased Sb–C bond length for the 2- and 6-substituted derivatives, averaged C–Sb–C angles for these compounds is also affected by steric bulk. The compounds 2,6-xylyl$_3$Sb (**1**) [45] (104.71(3)°), 2,4,6-mesityl$_3$Sb [73] (104.12(3)°), and (2,4,6-^{i}propyl$_3$-C$_6$H$_2$)$_3$Sb [74] (105.63(3)°) display much wider averaged C–Sb–C angles than, for example, the non-substituted phenyl$_3$Sb [63,64] (96.61(3)°) or even *o*-tolyl$_3$Sb [71] (97.22(3)°) and the related derivatives with substitution at the *ortho* position.

Table 1. List of selected bond lengths and angles and non-covalent interactions for selected triarylstibanes.

R_3Sb	Space Group	Sb–C (Å) (Avg.)	Edge to Face (Å)	C–Sb–C (°) (Avg.)	$CH_3\cdots\pi$ (Å)
phenyl$_3$Sb [63–68]	*P*-1	2.148(8)	2.89–3.37	96.61(3)	-
phenyl$_3$Sb [69]	$P2_1/c$	2.146(7)	2.97–3.23	96.34(3)	-
o-tolyl$_3$Sb [71]	*P*-1	2.164(6)	*	97.22(3)	*
m-tolyl$_3$Sb [65]	*Pbca*	2.148(3)	3.05	96.89(11)	3.28
p-tolyl$_3$Sb [70,75]	*R*-3	2.141(1)	2.89–3.31	97.33(3)	-
2,6-xylyl$_3$Sb (**1**) [45]	$P2_1/c$	2.190(2)	-	104.71(3)	2.82–3.18
(2,6-^{i}propyl$_2$-C$_6$H$_3$)$_3$Sb [76]	*I*-43*d*	2.176(7)	-	107.0(3)	3.29
2,4,6-mesityl$_3$Sb [73]	*P*-1	2.184(8)	-	104.12(3)	3.21
(2,4,6-^{i}propyl$_3$-C$_6$H$_2$)$_3$Sb [74]	*P*-1	2.184(8)	3.31	105.63(3)	3.26–3.35
1-naphthyl$_3$Sb·toluene (**2a**)	*P*-1	2.162(3)	2.76–2.81	96.87(3)	-
1-naphthyl$_3$Sb·benzene (**2b**)	*P*-1	2.162(2)	2.86–3.18	96.87(9)	-
9-phenanthrenyl$_3$Sb [72]	*P*-1	2.157(4)	2.81–2.86	96.77(1)	-
(2-phenyl-C$_6$H$_4$)$_3$Sb [77]	$P2_1/n$	2.165(2)	2.50–3.05	95.83(6)	-

* No hydrogen atoms reported.

All triarylstibanes display close packing motifs in the solid-state, creating 3D networks through the presence of non-covalent electrostatic interactions. Table 1 summarizes the non-covalent interactions in the presented triarylstibanes. With respect to the type of secondary non-covalent interactions in the extended solid state of triarylstibanes, clear trends begin to arise related to the substitution pattern of the aryl residue (Table 1). Unsurprisingly, phenyl$_3$Sb [63–69] only displays edge-to-face interactions (2.89–3.37 Å) due to the obvious lack of a methyl substituent or a polyaromatic residue. In addition to these electrostatic interactions between the aryl residues, phenyl$_3$Sb [63–69] also displays Sb$\cdots$C(π) interactions between the metal center and neighboring phenyl ring carbons (η^2 = 3.81, 3.95 Å). Sb$\cdots$C(π) interactions are within the sum of van der Waals for an Sb–C bond (4.24 Å) [78] and experimental cutoffs, as determined via a Cambridge Structural Database search (3.99 Å) [79]. No other triarylstibane displays Sb$\cdots$C(π) interactions, possibly due to the shielding effects of the more sterically hindered aryl residues. In

p-tolyl$_3$Sb [70], only edge-to-face interactions (2.89–3.31 Å) are observed despite the presence of a methyl substituent, which should lead to $CH_3\cdots\pi$ interactions. As expected, the addition of a methyl substituent at the *ortho* position results in the presence of $CH_3\cdots\pi$ interactions for 2,6-xylyl$_3$Sb (**1**) [45] (2.82–3.18 Å) (Figure 4), 2,4,6-mesityl$_3$Sb [73] (3.21 Å), and (2,4,6-^{i}propyl$_3$-C_6H_2)$_3$Sb [74] (3.26–3.35 Å). In both 1-naphthyl$_3$Sb·toluene (**2a**) and 1-naphthyl$_3$Sb·benzene (**2b**) (Figure 5), the bulkiness of all three naphthyl residues around the central antimony atom and the presence of cocrystallized solvent molecules does not allow for any $\pi\cdots\pi$ stacking interactions to be observed. However, edge-to-face interactions are observed between the naphthyl residues and both solvents benzene and toluene, 2.86–3.18 Å and 2.76–2.81 Å, respectively. 1-naphthyl$_3$Sb·toluene (**2a**) also displays $CH_3\cdots\pi$ interactions from the methyl group of toluene and neighboring naphthyl residues (2.77–2.86 Å). 9-phenanthrenyl$_3$Sb [72] also only displays edge-to-face interactions (2.81–2.86 Å).

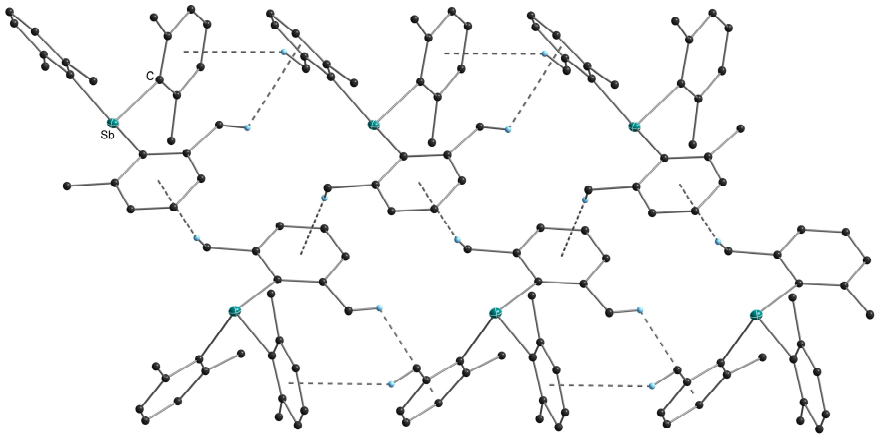

Figure 4. Crystal packing diagram for 2,6-xylyl$_3$Sb (**1**). $CH_3\cdots\pi$ interactions are highlighted with dashed bonds. All non-carbon atoms are shown as 30%-shaded ellipsoids. Edge-to-face interactions and hydrogen atoms that are not involved in intermolecular interactions are removed for clarity.

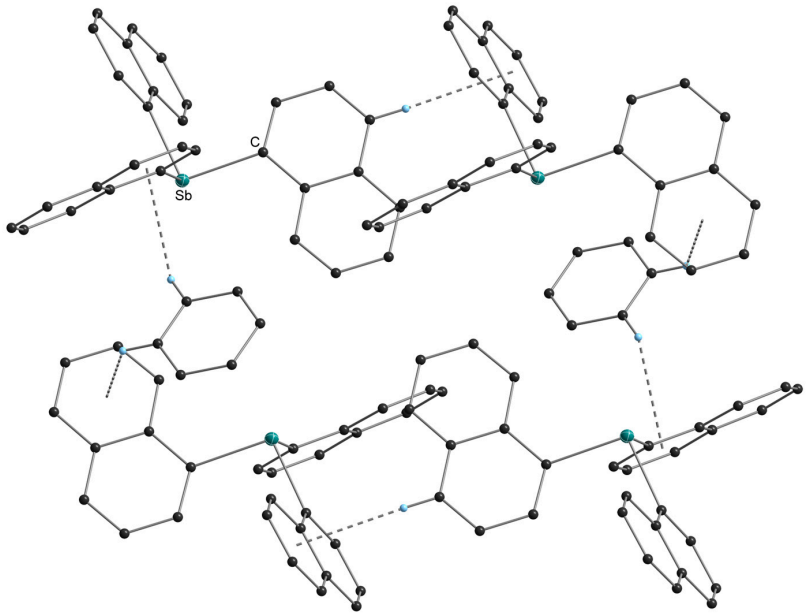

Figure 5. Crystal packing diagram for 1-naphthyl$_3$Sb·benzene (**2b**). Edge-to-face interactions are highlighted with dashed bonds. All non-carbon atoms are shown as 30%-shaded ellipsoids. Hydrogen atoms that are not involved in intermolecular interactions are removed for clarity.

2.2.2. Diarylantimony Bromides or R_2SbBr

As was observed for the triarylstibanes, the substitution pattern on the aryl residue and, hence, the steric bulk, the aryl residue affords the antimony metal center and has a marked effect on the Sb–C bond (Table 2). Similar to the triarylstibane derivatives, the shortest averaged Sb–C bond lengths are observed for compounds with aryl residues that are not substituted as in phenyl$_2$SbBr [49] (2.146(1) Å) or with substitution on only one *ortho* position as in 1-naphthyl$_2$SbBr [80] (2.151(8) Å). As expected, additional substitution at both *ortho* positions, as seen for 2,6-xylyl$_2$SbBr (**3**) (2.171(7) Å) and 9-anthracenyl$_2$SbBr·toluene (**5**) (2.183(14) Å), leads to a longer Sb–C bond. However, *ortho* substitution by a phenyl group in (2,6-phenyl$_2$-C_6H_3)$_2$SbBr [81] leads to the longest Sb–C bond (2.186(3) Å). In contrast, the Sb–Br bond lengths do not seem to follow this trend. Counterintuitively, 2,6-xylyl$_2$SbBr (**3**) displays the shortest Sb–Br bond length of 2.465(1) Å. However, considering the Lewis acidic nature of the antimony metal, which necessitates the presence of secondary interactions to help coordinatively saturate the metal center, this shortened and, thus, stronger bond length is not surprising in the absence of Sb···C(π) interactions, as in the case of 2,6-xylyl$_2$SbBr (**3**).

Table 2. List of selected bond lengths and angles for selected diarylantimony bromides.

R_2SbBr	Space Group	Sb–C (Å) (Avg.)	Sb–Br (Å)	C–Sb–C (°)	C–Sb–Br (°) (Avg.)
phenyl$_2$SbBr [49]	$P2_1/c$	2.146(1)	2.552(1)	98.5(3)	94.4(2)
2,6-xylyl$_2$SbBr (**3**)	$P2_1/n$	2.171(7)	2.465(1)	101.5(3)	99.22(2)
(2,6-phenyl$_2$-C_6H_3)$_2$SbBr [81]	$P2_1/n$	2.186(3)	2.5653(7)	99.4(1)	106.21(8)
1-naphthyl$_2$SbBr [80]	$P2_1/c$	2.151(8)	2.512(9)	98.0(2)	94.9(1)
9-anthracenyl$_2$SbBr·toluene (**5**)	$P2_1/c$	2.183(14)	2.566(2)	105.19(5)	95.74(4)

Despite all diarylantimony bromide derivatives crystallizing in the same monoclinic system, not all crystallize in the same space group, with 2,6-xylyl$_2$SbBr (**3**) (Figure 6) and (2,6-phenyl$_2$-C_6H_3)$_2$SbBr [81] crystallizing in the $P2_1/n$ space group (Table 3), perhaps due to both having rotating groups at the *ortho* positions. Concurrent with the only aryl residue with methyl groups on the aryl ring, 2,6-xylyl$_2$SbBr (**3**) displays a much different behavior in the solid state. This is due to the marked difference between the non-covalent interactions that the 2,6-xylyl residue can afford as compared to the phenyl, naphthyl, and anthracenyl residues, which behave as planar aromatic systems. By replacing one of the aryl residues with bromine, phenyl$_2$SbBr (d = 3.56 Å, R = 2.05 Å) [49], 1-naphthyl$_2$SbBr (d = 3.54 Å, R = 2.11 Å) [80], and 9-anthracenyl$_2$SbBr·toluene (**5**) (d = 3.47 Å, R = 1.07 Å) (Figure 7) all show close π···π stacking interactions between neighboring aromatic systems, creating extended 3D networks. In contrast, the methyl substituents on the aryl residue of 2,6-xylyl$_2$SbBr (**3**) allow for the molecules to orient themselves in order to maximize CH_3···π interactions. In all diarylantimony bromides, edge-to-face interactions are present and aid in propagating 3D networks. Curiously, 2,6-xylyl$_2$SbBr (**3**) is the only diarylantimony bromide to allow a Br···Br contact of 3.45 Å. This Br···Br contact is below the sum of van der Waals for a Br–Br bond (3.72 Å) [78] and below the experimental cutoffs, as determined via a Cambridge Structural Database search (3.79 Å) [79].

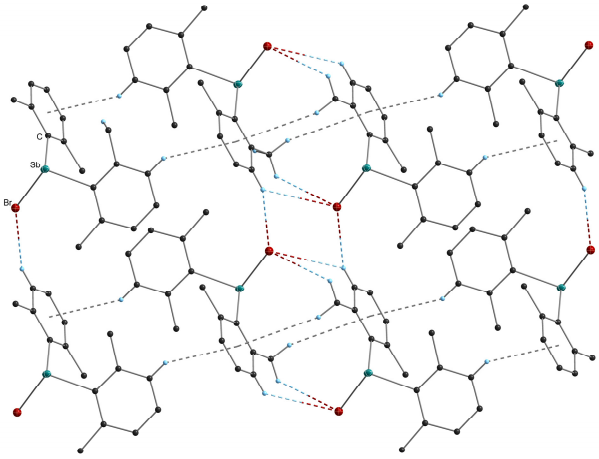

Figure 6. Crystal packing diagram for 2,6-xylyl$_2$SbBr (**3**). $CH_3\cdots\pi$ interactions, edge-to-face interactions, and C–H···Br contacts are highlighted with dashed bonds. All non-carbon atoms are shown as 30%-shaded ellipsoids. Hydrogen atoms that are not involved in intermolecular interactions are removed for clarity.

Table 3. List of non-covalent interactions for selected diarylantimony bromides.

R_2SbBr	π···π Stacking (Å)		Edge to Face (Å)	$CH_3\cdots\pi$ (Å)	C–H···Br (Å)	Sb···C(π) * (Å)
	d	R				
phenyl$_2$SbBr [49]	3.56	2.05	3.22	-	3.08–3.56	η^2 = 3.62–3.65
2,6-xylyl$_2$SbBr (**3**)	-	-	3.11	3.44	3.07–3.41	-
(2,6-phenyl$_2$-C_6H_3)$_2$SbBr [81]	-	-	2.73–3.27	-	2.53–3.55	-
1-naphthyl$_2$SbBr [80]	-	-	2.93–3.07	-	2.96–3.01	-
9-anthracenyl$_2$SbBr·toluene (**5**)	-	-	2.99–3.22	-	3.01–3.53	η^3 = 3.68–3.78

* Intermolecular interactions.

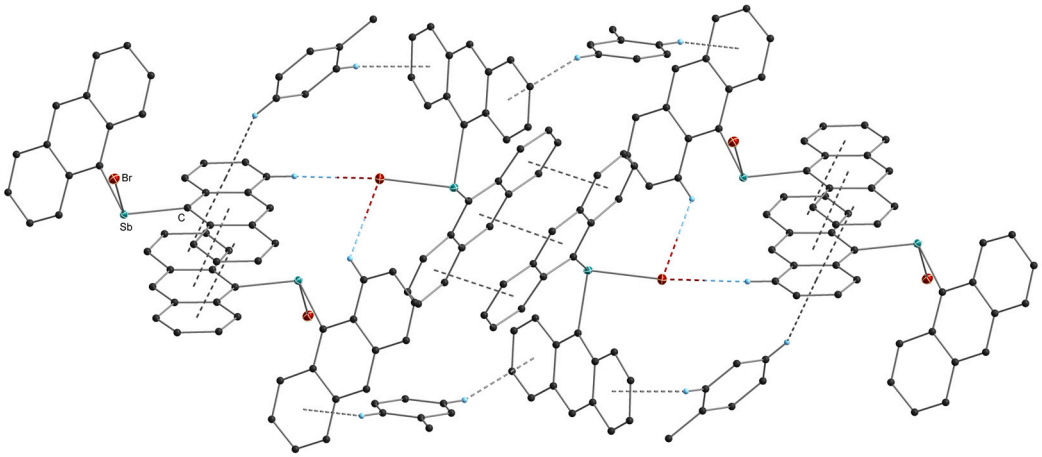

Figure 7. Crystal packing diagram for 9-anthracenyl$_2$SbBr·toluene (**5**). π–π stacking, edge-to-face interactions, and C–H···Br contacts are highlighted with dashed bonds. All non-carbon atoms are shown as 30%-shaded ellipsoids. Hydrogen atoms that are not involved in intermolecular interactions are removed for clarity.

In agreement with the increased Lewis acidity of the diarylantimony bromides as compared to the triarylstibanes, a higher propensity for Sb···C(π) interactions is observed. Phenyl$_2$SbBr [49] displays the closest Sb···C(π) interactions (η^2 = 3.63–3.65 Å) followed by 9-anthracenyl$_2$SbBr·toluene (**5**) (η^3 = 3.68–3.78 Å), with 2,6-xylyl$_2$SbBr (**3**) preferring the aforementioned Br···Br contact. However, in contrast to the well-known Menshutkin

complexes [82], no appreciable Sb···Br secondary contacts are observed, with all values (4.49–4.56 Å) being above the sum of van der Waals for an Sb–Br bond (4.33 Å) [78] and well above the experimental cutoffs, as determined via a Cambridge Structural Database search (3.84 Å) [79]. In addition to the electrostatic interactions described above, all the diarylantimony bromide derivatives display van der Waals interactions from the bromide substituent and hydrogens (C–H···Br) from neighboring molecules (Table 3).

2.2.3. Arylantimony Dichlorides or $RSbCl_2$

Despite the increased steric bulk afforded to the antimony metal by methyl substitution at the *ortho* position of the aryl residue, the Sb–C bonds are quite comparable for o-tolylSbCl$_2$ (**4**) (2.159(17) Å) as compared to phenylSbCl$_2$ [62] (2.151(2) Å) and p-tolylSbCl$_2$ [49] (2.148(6) Å) (Table 4). In addition, no appreciable deviations are observed for the Sb–Cl bond lengths, which fall in a narrow range of 2.384(2)–2.411(2) Å. All C–Sb–Cl and Cl–Sb–Cl angles are comparable and unremarkable. However, the increased steric bulk afforded by terphenyl ligands results in longer range of Sb–Cl bond lengths (2.161(3)-2.197(5) Å. The longest Sb–Cl bond length (2.197(5) Å) is found in the mixed halide Ar*SbCl$_2$ [34].

Table 4. List of selected bond lengths and angles for selected arylantimony dichlorides.

$RSbCl_2$	Space Group	Sb–C (Å)	Sb–Cl (Å)	C–Sb–Cl (°) (Avg.)	Cl–Sb–Cl (°)
phenylSbCl$_2$ [62]	*P*-1	2.151(2)	2.411(2)	93.95(2)	94.35(6)
o-tolylSbCl$_2$ (**4**)	*P*-1	2.159(17)	2.384(2)	93.71(5)	95.070(16)
p-tolylSbCl$_2$ [49]	*P*-1	2.148(6)	2.384(2)	93.4(2)	94.05(7)
Ar^{Mes}SbCl$_2$ [83]	$P2_1$	2.161(3)	2.383(3)	99.505(8)	91.34(4)
Ar^{Dipp}SbCl$_2$ [34]	$P2_12_12_1$	2.165(5)	2.4182(13)	98.015(13)	96.81(5)
Ar^{Tripp}SbCl$_2$ [84]	*Pnma*	2.187(5)	2.365(3)	100.22(11)	94.43(12)
Ar*SbCl$_2$/I$_2$ [34]	*P*-1	2.197(5)	2.410(7)	96.1(3)	94.2(3)

Ar^{Dipp} = C_6H_3-2,6-Dipp$_2$; Dipp = C_6H_2-2,6-^{i}Pr$_2$; Ar^{Mes} = C_6H_3-2,6-Mes$_2$; Mes = C_6H_2-2,4,6-Me$_3$; Ar^{Tripp} = C_6H_3-2,6-Tripp$_2$; Tripp = C_6H_2-2,4,6-^{i}Pr$_3$; Ar* = C_6H_2-2,6-(CHPh$_2$)$_2$-4-^{i}Pr.

As compared to the diarylantimony derivatives, the replacement of a second aryl residue by a halide, as in the case for the arylantimony dichlorides, should cause an increase in the overall Lewis acidity of the antimony metal center. This increase in Lewis acidity forces the presence of additional secondary interactions to help coordinatively saturate the antimony metal center. And indeed, this is the case for the smaller arylantimony dichlorides phenylSbCl$_2$ [62], *o*-tolylSbCl$_2$ (**4**), and *p*-tolylSbCl$_2$ [49]. Not only do these arylantimony dichlorides show the presence of a higher number of Sb···C(π) interactions, as compared to the diarylantimony bromides (Table 5), but they also display close Sb···Cl secondary contacts, which the bromides did not exhibit. In each of these arylantimony dichlorides, the metal center is completely saturated through η^6-Sb···C(π) interactions, where the aryl residue is completely tilted towards the metal center in order to maximize these interactions. The closest interactions are observed for phenylSbCl$_2$ [62] (η^6 = 3.30–3.72 Å), followed by *o*-tolylSbCl$_2$ (**4**) (η^6 = 3.37–3.77 Å) and *p*-tolylSbCl$_2$ [49] (η^6 = 3.31–3.81 Å). In each case, two molecules face each other in order to allow the phenyl ring to saturate the antimony metal center of the neighboring molecule. These two molecules interact with the next two via Sb···Cl secondary contacts, creating a linear chain, with all values—3.44 for phenylSbCl$_2$ [62], 3.55 Å for *o*-tolylSbCl$_2$ (**4**) (Figure 8), and 3.43 Å *p*-tolylSbCl$_2$ [49]— being well below the sum of van der Waals for an Sb–Cl bond (4.29 Å) [78] and below the experimental cutoffs, as determined via a Cambridge Structural Database search (3.79 Å) [79].

Table 5. List of non-covalent interactions for selected arylantimony dichlorides.

$RSbCl_2$	π···π Stacking (Å)		Edge to Face (Å)	CH_3···π (Å)	C–H····Cl (Å)	Sb···Cl (Å)	Sb···C(π) * (Å)
	d	R					
phenylSbCl$_2$ [62]	3.47	1.28	-	-	2.79–3.01	3.44	η^6 = 3.30–3.72
o-tolylSbCl$_2$ (**4**)	-	-	-	2.89	2.93–3.28	3.55, 3.89	η^6 = 3.37–3.77
p-tolylSbCl$_2$ [49]	-	-	-	2.69	2.86–3.31	3.43, 3.64	η^6 = 3.31–3.81
Ar^{Mes}SbCl$_2$ [83]	-	-	2.78–2.80	-	2.73–3.08	3.41	-
Ar^{Dipp}SbCl$_2$ [34]	-	-	3.25	2.95	2.87–3.16	-	-
Ar^{Tripp}SbCl$_2$ [84]	-	-	-	2.76–3.01	2.34–3.34	-	-
Ar*SbCl$_2$ [34]	-	-	2.59–3.05	2.76	2.73	3.42	-

Ar^{Dipp} = C_6H_3-2,6-Dipp$_2$; Dipp = C_6H_2-2,6-^{i}Pr$_2$; Ar^{Mes} = C_6H_3-2,6-Mes$_2$; Mes = C_6H_2-2,4,6-Me$_3$; Ar^{Tripp} = C_6H_3-2,6-Tripp$_2$; Tripp = C_6H_2-2,4,6-^{i}Pr$_3$; Ar* = C_6H_2-2,6-(CHPh$_2$)$_2$-4-^{i}Pr; * intermolecular interactions.

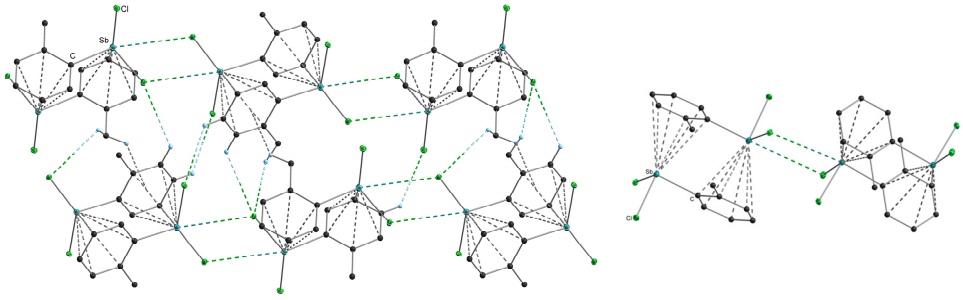

Figure 8. Crystal packing diagram for *o*-tolylSbCl$_2$ (**4**). Sb···C(π) and CH_3···π interactions and C–H···Cl contacts are highlighted with dashed bonds (**left**). Sb···C(π) interactions in *o*-tolylSbCl$_2$ (**4**) (**right**). All non-carbon atoms are shown as 30%-shaded ellipsoids. Edge-to-face interactions and hydrogen atoms that are not involved in intermolecular interactions are removed for clarity.

Both *o*-tolylSbCl$_2$ (**4**) and *p*-tolylSbCl$_2$ [49] subsequently display a second slightly longer Sb···Cl secondary contact (3.89 and 3.64 Å, respectively) through the exposed chloride substituent from one chain and the antimony metal center of the adjacent chain. An extended 3D network is then achieved with the help of both close CH_3···π interactions and C–H···Cl contacts. However, the absence of methyl substituents in phenylSbCl$_2$ [62] does not allow for CH_3···π interactions, and close π···π stacking interactions are present between the chains. This circumvents the presence of an additional Sb···Cl contact, as was observed for *o*-tolylSbCl$_2$ (**4**) and *p*-tolylSbCl$_2$ [49], but phenylSbCl$_2$ [62] displays the closest C–H···Cl contacts (2.79–3.01 Å) among these three arylantimony dichlorides, aiding in propagating an extended 3D network. Displaying the stabilizing strength and necessity of these Sb···C(π) secondary interactions, none of these arylantimony dichlorides derivatives display edge-to-face interactions.

In accordance with the increased steric bulk around the antimony metal center, the terphenyl derivatives Ar^{Mes}SbCl$_2$ [83], Ar^{Dipp}SbCl$_2$ [34], Ar^{Tripp}SbCl$_2$ [84], and Ar*SbCl$_2$ [34] do not display any Sb···C(π) secondary interactions. However, Ar^{Mes}SbCl$_2$ [83] (3.41 Å) and Ar*SbCl$_2$ [34] (3.42 Å) display similar Sb···Cl contacts, as was observed for the smaller residues; the steric bulk does not allow further contacts. As expected, close CH_3···π interactions and C–H···Cl contacts are observed through the terphenyl substituents between neighboring molecules in the extended solid state.

2.2.4. Diaryldistibanes or $[R_2Sb]_2$

Consistent with increased steric demand around the central antimony atom by aryl residues substituted at both the 2- and 6-positions, the longest average Sb–C bond lengths among the presented diaryldistibanes are observed for [(2,4,6-^{i}propyl$_3$-C_6H_2)$_2$Sb]$_2$ [85], with an averaged Sb–C bond length of 2.209(3), and [2,4,6-mesityl$_2$Sb]$_2$ [73,86] (2.199(8) Å), followed by [9-anthracenyl$_2$Sb]$_2$ (**6**), with an Sb–C bond length of 2.157(2) Å and longer as compared to 2.157(2) Å in [phenyl$_2$Sb]$_2$ (Table 6) [87,88]. A similar trend is observed

for Sb¬Sb bond lengths, as a slight increase in the Sb¬Sb bond lengths is observed for [9-anthracenyl$_2$Sb]$_2$ (**6**) (2.889(4) Å) and [2,4,6-mesityl$_2$Sb]$_2$ [73,86] (2.848(1) Å) as compared to 2.836(2) Å in [phenyl$_2$Sb]$_2$ [87,88]. In conjunction with the longer Sb¬Sb bond lengths for [9-anthracenyl$_2$Sb]$_2$ (**6**), the large sterically encumbering residue also displays the widest C¬Sb¬C angles, with an average value of 100.89(11)° as compared to [phenyl$_2$Sb]$_2$ [87,88], which displays much more narrower C¬Sb¬C angles of 94.36(1)° and C¬Sb¬Sb angles with an average value of 95.24(1)°.

Table 6. List of selected bond lengths and angles for selected diaryldistibanes.

[Rl$_2$Sb]$_2$	Space Group	Sb–Sb (Å)	Sb–C (Å) (Avg.)	C–Sb–C (°)	C–Sb–Sb (°)
[phenyl$_2$Sb]$_2$ [87,88]	$P2_1/n$	2.836(2)	2.157(2)	94.36(1)	93.78(1) 96.69(1)
[2,4,6-mesityl$_2$Sb]$_2$ [73,86]	$P2_1/n$	2.848(1)	2.199(8)	97.5(3) 100.8(3)	90.0(2) 109.5(2) 92.2(2) 108.7(2)
[(2,4,6-^{i}propyl$_3$-C$_6$H$_2$)$_2$Sb]$_2$ [85]	P-1	2.8587(6)	2.209(3)	95.89(13) 95.89(13)	91.27(9) 112.52(9) 90.79(1) 111.81(1)
[9-anthracenyl$_2$Sb]$_2$ (**6**)	$P2_1/c$	2.889(4)	2.187(3)	101.03(11) 100.76(11)	85.67(7) 102.87(8) 90.20(7) 111.73(8)

With respect to electrostatic interactions in the extended solid state, the diaryldistibanes exhibit expected interactions that are directly dependent on the nature of the aryl residue. In [phenyl$_2$Sb]$_2$ [87,88], consistent with the smaller planar aromatic residue, the phenyl groups along the Sb¬Sb bond do not face each other but rather orient themselves perpendicularly in order to afford short intramolecular edge-to-face interactions of 2.95 Å and also allow intermolecular edge-to-face interactions (3.17–3.34 Å), resulting in a 3D extended network (Table 7). In [2,4,6-mesityl$_2$Sb]$_2$ [73,86], in addition to intramolecular CH$_3$···π interactions of 3.19–3.34 Å, all three methyl substituents on the aryl residue interact intermolecularly through CH$_3$···π interactions (2.92–3.34 Å) with neighboring molecules. Intermolecular edge-to-face interactions aid in propagating an extended 3D network. Both intra- (2.65–2.96 Å) and intermolecular (2.72–2.84 Å) CH$_3$···π interactions with neighboring molecules are observed in [(2,4,6-^{i}propyl$_3$-C$_6$H$_2$)$_2$Sb]$_2$ [85]. Finally, the 9-anthracenyl residue displays π···π stacking interactions in [9-anthracenyl$_2$Sb]$_2$ (**6**) (Figure 9), although not with a neighboring molecule but rather intramolecularly with a 9-anthracenyl residue across the Sb¬Sb bond (d = 3.42 Å, R = 0.86 Å). Subsequently, neighboring molecules interact through edge-to-face interactions (2.69–3.23 Å), creating an extended 3D network.

Table 7. List of selected bond lengths and angles for selected diaryldistibanes.

[Rl$_2$Sb]$_2$	π···π Stacking (Å)		Edge to Face (Å)		CH$_3$···π (Å)	
	d	R	Intra	Inter	Intra	Inter
[phenyl$_2$Sb]$_2$ [87,88]	-	-	2.95	3.17–3.34	-	-
[2,4,6-mesityl$_2$Sb]$_2$ [73,86]	-	-	-	2.92–3.34	3.19–3.34	2.99
[(2,4,6-^{i}propyl$_3$-C$_6$H$_2$)$_2$Sb]$_2$ [85]	-	-	-	-	2.65–2.96	2.72–2.84
[9-anthracenyl$_2$Sb]$_2$ (**6**)	3.42 (intra)	0.86 (intra)	-	2.69–3.23	-	-

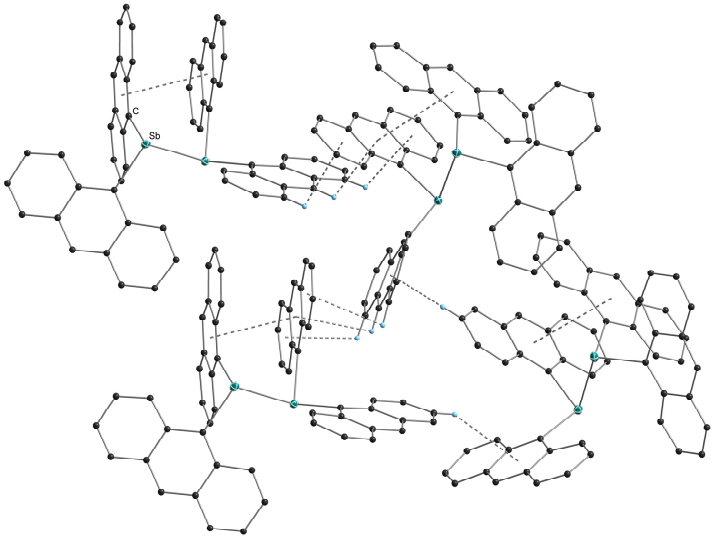

Figure 9. Crystal packing diagram for [9-anthracenyl$_2$Sb]$_2$ (**6**). π···π stacking and edge-to-face interactions are highlighted with dashed bonds. All non-carbon atoms are shown as 30%-shaded ellipsoids. Hydrogen atoms that are not involved in intermolecular interactions are removed for clarity.

3. Materials and Methods

3.1. Materials and Methods

All reactions, unless otherwise stated, were carried out using standard Schlenk line techniques under a nitrogen atmosphere or in a nitrogen-flushed glovebox UNILAB (M. Braun Inertgassystems GmbH, Garching, Germany). All dried and deoxygenated solvents were obtained from a solvent drying system, PureSolve MD5 (Innovative Technology Inc., Amesbury, MA, USA). $SbCl_3$ anhydrous (98% *v*/*v*) was purchased at Alfa Aesar, sublimed, and stored under nitrogen. All other chemicals from commercial sources (arylbromides, ^{n}BuLi, and $SbBr_3$) were utilized without further purification. The preparation of *o*-tolylSbCl$_2$ (**4**) followed the literature procedure [43]. Elemental analysis was performed with an Elementar Vario EL III (Elementar Analysensysteme GmbH, Langenselbold, Germany). Melting point measurements were carried out via threefold determination with a Stuart Scientific SMP 10 (Norrscope Ltd., Chelmsford, UK) (up to 300 °C).

3.1.1. NMR Spectroscopy

^{1}H (300.22 MHz) and ^{13}C (75.5 MHz) spectra were recorded on a Mercury 300 MHz spectrometer from Varian, Inc. (Palo Alto, CA, USA) at 25 °C. Chemical shifts for ^{1}H and ^{13}C were recorded in parts per million with $CDCl_3$ (7.26 ppm for ^{1}H or 77.0 ppm for ^{13}C) as a reference.

3.1.2. Single-Crystal X-ray Diffraction

All crystals suitable for single-crystal X-ray diffractometry were removed from a vial or a Schlenk under N_2 and immediately covered with a layer of silicone oil. A single crystal was selected, mounted on a glass rod on a copper pin, and placed in the cold N_2 stream provided with an Oxford 700 Cryometer (Oxford Cryosystems, Oxford, UK). XRD data collection was performed on a Bruker APEX II diffractometer (Bruker AXS Advanced Xray Solutions GmbH, Karlsruhe, Germany) [89] with use of an Incoatec microfocus sealed tube with Mo Kα radiation (λ= 0.71073 Å) and a CCD area detector. Empirical absorption corrections were applied using SADABS or TWINABS [90–92]. The structures were solved with the use of the intrinsic phasing option in SHELXT [93] and refined using the full-matrix least-squares procedures in SHELXL [93–97], as implemented in the program SHELXLE [98]. The space group assignments and structural solutions were evaluated using PLATON [99,100]. Non-hydrogen atoms were refined anisotropically. All hydrogen atoms were located in calculated positions corresponding to standard bond lengths and angles

and refined using a riding model. The disorder observed in the solvent of crystallization toluene in 1-naphthyl$_3$Sb·toluene (**2a**) was handled by modeling the occupancies of the individual orientations using free variables to refine the respective occupancy of the affected fragments (PART) [101]. Disordered positions for the solvent of crystallization toluene in 1-naphthyl$_3$Sb·toluene (**2a**) were refined using 50/50 split positions with additional restraints to afford optimized geometries (FLAT and AFIX 66). The rigid-bond restraint DELU was used in modeling disorder to make the ADP values of the disordered atoms more reasonable. The residual electron density around the bromine atom in 2,6-xylyl$_2$SbBr (**3**) is attributed to possible substitutional disorder. During the synthesis of these species, a mixture of the bromine and chlorine derivatives is observed, and they are difficult to separate. Any attempts to resolve this disorder resulted in unstable refinements. Electrostatic non-covalent intermolecular interactions [50–54], van der Waals contacts (C–H···X) [55–60], and secondary contacts with antimony (Sb···C(π), Sb···X) [49,61,62] for the presented and published compounds were based on a Cambridge Structural Database [79] search and fall within expected ranges. Centroids and planes were determined by features of the programs Mercury [102] and Diamond [103]. All crystal structures representations were made with the program Diamond [103]. Details about measurements and crystallographic data are provided in the Supporting Information for this article.

3.2. Syntheses

3.2.1. General Procedure for Compounds **1**–**3** and **5**–**6**

A flask equipped with a dropping funnel and a reflux condenser was charged with Mg in THF. The dropping funnel was charged with arylbromide in THF, about 10% of the solution was added to the reaction vessel, and the solution was heated carefully, or dibromoethane was added to start the reaction. The arylbromide was subsequently added dropwise. After complete addition, the reaction was refluxed for 3 to 12 h. Residual Mg was filtered off using a filter cannula. The filtered solution was then added to a solution of $SbCl_3$ in THF cooled to 0 °C. The solution was stirred overnight at room temperature. After the removal of THF, toluene was added, and the liquid was filtered using a cannula. Toluene was removed under reduced pressure, and the product was recrystallized.

2,6-xylyl$_3$Sb (1): 4.01 g (165 mmol, 3.30 eq.) Mg in 50 mL THF, 27.8 g (150 mmol, 3.00 eq.) 1-bromo-2,6-dimethylbenzene in ml THF, and 10.0 g (50.0 mmol, 1.00 eq.) $SbCl_3$ in 50 mL THF at 0 °C. The resulting solid was recrystallized from toluene at −30 °C to obtain light yellow crystals. Yield: 45%. M.p.: 121 °C. Elemental analysis (%) for $C_{24}H_{27}Sb$: C, 65.93; H, 6.22. Found: C, 64.88; H, 6.18. ^{1}H NMR (C_6D_6, 300 MHz): δ 6.90 (t, 3H, ArH), 6.73 (d, 6H, ArH), 2.35 (s, 18H, CH_3). ^{13}C NMR ($CDCl_3$, 75.5 MHz): δ 143.75, 142.05, 129.70, 128.66, 24.40 (CH_3) ppm.

1-naphthyl$_3$Sb (2): 2.00 g (82.3 mmol, 4.20 eq.) Mg in 100 mL THF, 15.5 g (74.9 mmol, 3.80 eq.) 1-bromonaphthalene in 50 mL THF, and 4.50 g (19.7 mmol, 1.00 eq.) $SbCl_3$ in 60 mL THF at 0 °C. The resulting solid was recrystallized from toluene (**2a**) or benzene (**2b**) or at −30 °C to obtain colorless crystals. Yield: 65%. M.p.: 222 °C. Elemental analysis (%) for $C_{30}H_{21}Sb$: C, 71.60; H, 4.21. Found: C, 74.06; H, 4.43. ^{1}H NMR ($CDCl_3$, 300 MHz): δ 8.18 (d, 3H, ArH), 7.84 (d, 6H, ArH), 7.46 (m, 6H, ArH), 7.29 (d, 3H, ArH), 7.18 (d, 3H, ArH) ppm. ^{13}C NMR ($CDCl_3$, 75.5 MHz): δ 138.00, 136.51, 136.24, 133.85, 129.40, 129.31, 129.90, 126.30, 126.29, 125.85 ppm.

2,6-xylyl$_2$SbBr (3): 1.04 g (42.8 mmol, 1.34 eq.) Mg in 100 mL THF, 7.00 g (37.8 mmol, 1.20 eq.) 1-bromo-2,6-dimethylbenzene in 30 mL THF, and 7.18 g (31.5 mmol, 1.00 eq.) $SbCl_3$ in 100 mL THF at 0 °C. The resulting solid was recrystallized from toluene at −30 °C to obtain light yellow crystals. Yield: 55%. Alternative: A solution of 0.37 g $SbCl_3$ (1.60 mmol, 1.00 eq.) in dry Et_2O was added dropwise to a stirred solution of 1.40 g 2,6-xylyl$_3$Sb (1) (3.20 mmol, 1.00 eq.) in Et_2O. The solution was refluxed for 4 h and stirred at room temperature overnight. After the removal of the solvent, colorless crystals were obtained upon recrystallization from toluene at −30 °C. M.p.: 82 °C. Elemental analysis (%) for $C_{16}H_{18}SbBr$: C, 46.65; H, 4.40. Found: C, 49.70; H, 4.52. ^{1}H NMR ($CDCl_3$, 300 MHz):

δ 7.15 (t, 2H, ArH), 7.03 (d, 4H, ArH), 2.43 (s, 12H, CH_3) ppm. ^{13}C NMR ($CDCl_3$, 75.5 MHz): δ 144.35, 143.73, 143.66, 142.05, 129.70, 128.66, 25.01 (CH_3), 24.39 (CH_3) ppm.

9-anthracenyl$_2$SbBr (5): 0.85 g (35.0 mmol, 4.10 eq.) Mg in 80 mL THF, 8.17 g (31.8 mmol, 3.70 eq.) 9-bromoanthracene in 30 mL THF, and 1.94 g (8.50 mmol, 1.00 eq.) $SbCl_3$ in 40 mL THF at 0 °C. The resulting solid was recrystallized from toluene and pentane at −30 °C to obtain yellow crystals. Yield: 45%. M.p.: 222 °C. Elemental analysis (%) for $C_{28}H_{18}SbBr$: C, 60.47; H, 3.26. Found: C, 64.37; H, 3.53. ^{1}H NMR ($CDCl_3$, 300 MHz): δ 8.53 (s, 4H), 8.00 (d, 4H), 7.94 (d, 4H), 7.40 (d, 4H), 7.17 (s, 2H) ppm. ^{13}C NMR ($CDCl_3$, 75.5 MHz): δ 131.66, 130.39, 129.31, 128.13, 126.18, 126.67, 1225.30, 124.74 ppm.

[9-anthracenyl$_2$Sb]$_2$ (6): 0.61 g (25.0 mmol, 4.10 eq.) Mg in 60 mL THF, 5.79 g (22.5 mmol, 3.70 eq.) 9-bromoanthracene in 20 mL THF, and 2.20 g (6.09 mmol, 1.00 eq.) $SbBr_3$ in 40 mL THF at 0 °C. The resulting solid was recrystallized from toluene and pentane at −30 °C to obtain orange crystals. Yield: 33%. M.p.: 231 °C. Elemental analysis (%) for $C_{56}H_{36}Sb_2$: C, 70.62; H, 3.81. Found: C 69.45; H, 3.81. ^{1}H NMR ($CDCl_3$, 300 MHz): δ 8.42 (d, 8H, ArH), 7.86 (s, 4H, ArH), 7.61 (d, 8H, ArH), 7.10 (t, 8H, ArH), 6.81 (t, 8H, ArH) ppm. ^{13}C NMR ($CDCl_3$, 75.5 MHz): δ 138.41, 136.41, 131.15, 130.98, 129.26, 128.29, 125.33, 124.30 ppm.

3.2.2. Synthesis of (**4**)

***o*-tolylSbCl$_2$ (4) [43]**: A solution of 9.12 g $SbCl_3$ (40.0 mmol, 2.00 eq.) in dry Et_2O was added dropwise to a stirred solution of 7.90 g *o*-tolyl$_3$Sb (20.0 mmol, 1.00 eq.) in Et_2O. The solution was refluxed for 4 h and stirred at room temperature overnight. After the removal of the solvent, colorless crystals were obtained upon recrystallization from a mixture of toluene and heptane. Yield: 58%. Mp: 105 °C. Elemental analysis (%) for $C_7H_7SbCl_2$: C, 29.63; H, 2.49. Found: C, 29.78; H, 2.43. ^{1}H NMR ($CDCl_3$, 300 MHz): δ 8.15 (d, 1H, ArH), 7.44 (m, 2H, ArH), 7.27 (d, 1H, ArH), 2.65 (s, 3H, CH_3). ^{13}C NMR ($CDCl_3$, 75.5 MHz): δ 149.94, 141.62, 133.00, 131.72, 130.81, 127.64, 22.09 (CH_3) ppm.

Supplementary Materials: The following supporting information can be downloaded at: https://www.mdpi.com/article/10.3390/cryst14100860/s1, Figure S1: ^{1}H NMR spectrum of 2,6-xylyl$_3$Sb (**1**) in C_6D_6; Figure S2: {^{1}H}13C NMR spectrum of 2,6-xylyl$_3$Sb (**1**) in $CDCl_3$; Figure S3: ^{1}H NMR spectrum of 1-naphthyl$_3$Sb (**2**) in $CDCl_3$; Figure S4: {^{1}H}13C NMR spectrum of 1-naphthyl$_3$Sb (**2**) in $CDCl_3$; Figure S5: ^{1}H NMR spectrum of 2,6-xylyl$_2$SbBr (**3**) in $CDCl_3$; Figure S6: {^{1}H}13C NMR spectrum of 2,6-xylyl$_2$SbBr (**3**) in $CDCl_3$; Figure S7: ^{1}H NMR spectrum of 9-anthracenyl$_2$SbBr (**5**) in $CDCl_3$; Figure S8: {^{1}H}^{13}C NMR spectrum of 9-anthracenyl$_2$SbBr (**5**) in $CDCl_3$; Figure S9: {^{1}H}^{13}C NMR spectrum of [9-anthracenyl$_2$Sb]$_2$ (**6**) in $CDCl_3$; Figure S10: ^{1}H NMR spectrum of $_2$ (**6**) in $CDCl_3$; Figure S11: ^{1}H NMR spectrum of o-tolylSbCl$_2$ (**4**) in C_6D_6; Figure S12: {^{1}H}^{13}C NMR spectrum of o-tolylSbCl$_2$ (**4**) in $CDCl_3$; Table S1: Crystallographic data and details of measurements for compound (**1**–**6**).

Author Contributions: Conceptualization, M.W. and F.U.; Formal analysis, A.T. and M.W.; Investigation, M.W. and R.C.F.; Methodology, M.W.; Supervision, F.U.; Validation, A.T.; Visualization, A.T.; Writing—original draft, A.T. and M.W.; Writing—review and editing, A.T. All authors have read and agreed to the published version of the manuscript.

Funding: This research received no external funding.

Data Availability Statement: The spectroscopic data and tabulated crystallographic data presented in this study are included in the Supplementary Materials, which can be accessed online. The deposition numbers 1828581-1828587 contain the supplementary crystallographic data for this article. The data are provided free of charge by the joint Cambridge Crystallographic Data Centre and Fachinformationszentrum Karlsruhe Access Structures service (www.ccdc.cam.ac.uk/structures) (accessed on 24 September 2024).

Acknowledgments: We thank NAWI Graz, a collaboration between Graz University of Technology and the University of Graz.

Conflicts of Interest: The authors declare no conflicts of interest.

References

1. Loewig. Schweitzer, Organic bases containing antimony. *J. Pr. Chem.* **1853**, *XLIX*, 385.
2. Cho, C.S.; Motofusa, S.-I.; Ohe, K.; Uemura, S. Palladium(II)-catalyzed conjugate addition of aromatics to α,β-unsaturated ketones and aldehydes with arylantimony compounds. *Bull. Chem. Soc. Jpn.* **1996**, *69*, 2341–2348. [CrossRef]
3. Cho, C.S.; Tanabe, K.; Itoh, O.; Uemura, S. Facile Palladium-Catalyzed Carbonylation of Triarylstibines in the Presence of Ammonium Cerium(IV) Nitrate. *J. Org. Chem.* **1995**, *60*, 274–275. [CrossRef]
4. Cho, C.S.; Tanabe, K.; Uemura, S. Palladium(II)-catalyzed hydroarylation of α,β-unsaturated aldehydes and ketones with triarylstibines in the presence of silver acetate. *Tetrahedron Lett.* **1994**, *35*, 1275–1278. [CrossRef]
5. Freedman, L.D.; Doak, G.O. Antimony: Annual survey covering the year 1993. *J. Organomet. Chem.* **1995**, *496*, 137–152. [CrossRef]
6. Huang, Y. Synthetic applications of organoantimony compounds. *Acc. Chem. Res.* **1992**, *25*, 182–187. [CrossRef]
7. Kakusawa, N.; Tsuchiya, T.; Kurita, J. Photochemically induced coupling reaction of triarylstibines with olefins. *Tetrahedron Lett.* **1998**, *39*, 9743–9746. [CrossRef]
8. Kakusawa, N.; Yamaguchi, K.; Kurita, J.; Tsuchiya, T. Palladium-catalyzed cross-coupling reactions between 1-alkynylstibines and acyl chlorides. *Tetrahedron Lett.* **2000**, *41*, 4143–4146. [CrossRef]
9. Matoba, K.; Motofusa, S.-I.; Cho, C.S.; Ohe, K.; Uemura, S. Palladium(II)-catalyzed phenylation of unsaturated compounds using phenylantimony chlorides under air. *J. Organomet. Chem.* **1999**, *574*, 3–10. [CrossRef]
10. Yasuike, S.; Okajima, S.; Kurita, J. Synthesis of optically active organoantimony compounds having an (S)-α-methylbenzyldimethylamine group and its evaluation for asymmetric reaction. *Chem. Pharm. Bull.* **2002**, *50*, 1404–1406. [CrossRef]
11. Yasuike, S.; Okajima, S.; Yamaguchi, K.; Seki, H.; Kurita, J. Synthesis and resolution of 2,2′-bis[di(p-tolyl)stibano]-1,1′-binaphthyl (BINASb); the first example of an optically active organoantimony ligand for asymmetric synthesis. *Tetrahedron Asymmetry* **2000**, *11*, 4043–4047. [CrossRef]
12. Yasuike, S.; Okajima, S.; Yamaguchi, K.; Seki, H.; Kurita, J. New optically active organoantimony (BINASb) and bismuth (BINABi) compounds comprising a 1,1′-binaphthyl core: Synthesis and their use in transition metal-catalyzed asymmetric hydrosilylation of ketones. *Tetrahedron* **2003**, *59*, 4959–4966. [CrossRef]
13. Schulz, S. Covalently bonded compounds of heavy group 15/16 elements-Synthesis, structure and potential application in material sciences. *Coord. Chem. Rev.* **2015**, *297*, 49–76. [CrossRef]
14. Freedman, L.D.; Doak, G.O. *The Use of Organoantimony and Organobismuth Compounds in Organic Synthesis*; Wiley: Hoboken, NJ, USA, 1989; pp. 397–433.
15. Cullen, W.R.; Wu, A.W. The reaction of 1,2-dilithiotetrafluorobenzene with Group V halides. *J. Fluorine Chem.* **1976**, *8*, 183–187. [CrossRef]
16. Ashe, A.J., III; Kampf, J.W.; Al-Taweel, S.M. Conformations of heteroferrocenes. Synthesis and crystal and dynamic solution behavior of 2,2′,5,5′-tetrakis(trimethylsilyl)-3,3′,4,4′-tetramethyl-1,1′-distibaferrocene. *Organometallics* **1992**, *11*, 1491–1496. [CrossRef]
17. Naumann, D.; Tyrra, W.; Leifeld, F. Polar trifluoromethylation reactions. Synthesis and NMR spectra of tris(trifluoromethyl)antimony, $Sb(CF_3)_3$. *J. Organomet. Chem.* **1987**, *333*, 193–197. [CrossRef]
18. Ganja, E.A.; Ontiveros, C.D.; Morrison, J.A. Preparation of bis(trifluoromethyl)tellurium, bis(trifluoromethyl)selenium, bis(trifluoromethyl)diselenium, tris(trifluoromethyl)antimony, tris(trifluoromethyl)arsine, bis(trifluoromethyl)arsenic iodide, tris(trifluoromethyl)phosphine, and (trifluoromethyl)phosphorus diiodide by reaction of bis(trifluoromethyl)mercury with the Group 5 and 6A (15 and 16) halides. *Inorg. Chem.* **1988**, *27*, 4535–4538. [CrossRef]
19. Ates, M.; Breunig, H.J.; Soltani-Neshan, A.; Tegeler, M. Synthesis of mesitylstibines. *Z. Naturforsch. B Anorg. Chem. Org. Chem.* **1986**, *41*, 321–326. [CrossRef]
20. Opris, L.M.; Silvestru, A.; Silvestru, C.; Breunig, H.J.; Lork, E. Solid-state structure and solution behaviour of hypervalent organoantimony halides containing 2-$(Me_2NCH_2)C_6H_4$-moieties. *Dalton Trans.* **2003**, *22*, 4367–4374. [CrossRef]
21. Wieber, M.; Wirth, D.; Fetzer, I. New synthesis methods for organohalostibines. *Z. Anorg. Allg. Chem.* **1983**, *505*, 134–137. [CrossRef]
22. Kakusawa, N.; Ikeda, T.; Osada, A.; Kurita, J.; Tsuchiya, T. Synthesis of Sb-chiral organoantimony(III) compounds: Stepwise nucleophilic displacement reaction of tribromostibane via a bisethynylstibane intermediate. *Synlett* **2000**, *2000*, 1503–1505. [CrossRef]
23. Garje, S.S.; Jain, V.K. The chemistry of organo-arsenic, antimony and bismuth compounds: An overview. *Main Group Met. Chem.* **1999**, *22*, 45–58. [CrossRef]
24. Nunn, M.; Sowerby, D.B.; Wesolek, D.M. The preparation of phenyl substituted antimony(III) and antimony(V) chlorides and bromides. *J. Organomet. Chem.* **1983**, *251*, C45–C46. [CrossRef]
25. Breunig, H.J.; Roesler, R. Organoantimony compounds with element-element bonds. *Coord. Chem. Rev.* **1997**, *163*, 33–53. [CrossRef]
26. Balazs, L.; Breunig, H.J. Organometallic compounds with Sb-Sb or Bi-Bi bonds. *Coord. Chem. Rev.* **2004**, *248*, 603–621. [CrossRef]
27. Breunig, H.J.; Ghesner, I. Coordination compounds with organoantimony and Sbn ligands. *Adv. Organomet. Chem.* **2003**, *49*, 95–131. [CrossRef]
28. Paneth, F.A. Use of free methyl and ethyl in chemical synthesis. *Trans. Faraday Soc.* **1934**, *30*, 179–181. [CrossRef]

29. Li, Y.-Z.; Ganguly, R.; Leong, W.K. Oxidative Addition across Sb-H and Sb-Sb Bonds by an Osmium Carbonyl Cluster: Trapping the Intermediate. *Organometallics* **2014**, *33*, 823–828. [CrossRef]
30. Hendershot, D.G.; Pazik, J.C.; Berry, A.D. Synthesis, characterization, and chemical vapor deposition properties of primary and secondary neopentylstibine. New antimony precursors for MOCVD. *Chem. Mater.* **1992**, *4*, 833. [CrossRef]
31. Twamley, B.; Hwang, C.-S.; Hardman, N.J.; Power, P.P. Sterically encumbered terphenyl substituted primary pnictanes $ArEH_2$ and their metallated derivatives ArE(H)Li (Ar= C_6H_3-2,6-$Trip_2$; Trip=2,4,6-triisopropylphenyl; E=N, P, As, Sb). *J. Organomet. Chem.* **2000**, *609*, 152–160. [CrossRef]
32. Breunig, H.J.; Lork, E.; Moldovan, O.; Raţ, C.I. Syntheses of a stable tristibine and of related antimony compounds with the 2,6-dimesitylphenyl (Dmp) substituent. *J. Organomet. Chem.* **2008**, *693*, 2527–2534. [CrossRef]
33. Olaru, M.; Duvinage, D.; Lork, E.; Mebs, S.; Beckmann, J. Heavy Carbene Analogues: Donor-Free Bismuthenium and Stibenium Ions. *Angew. Chem., Int. Ed.* **2018**, *57*, 10080–10084. [CrossRef] [PubMed]
34. Roller, C.A.; Doler, B.; Steller, B.G.; Saf, R.; Fischer, R.C. A Distibene with Extremely Long Sb=Sb Distance and Related Heavier Dipnictenes from Salt-Free Metathesis Reactions. *Eur. J. Inorg. Chem.* **2023**, *27*, e202300586. [CrossRef]
35. Cowley, A.H.; Jones, R.A.; Nunn, C.M.; Westmoreland, D.L. $[Mes_2SbCu(PMe_3)_2]_2$: The First CuI Antimonide. *Angew. Chem. Int. Ed.* **1989**, *28*, 1018–1019. [CrossRef]
36. Pang, Y.; Leutzsch, M.; Nöthling, N.; Cornella, J. Dihydrogen and Ethylene Activation by a Sterically Distorted Distibene. *Angew. Chem., Int. Ed.* **2023**, *62*, e202302071. [CrossRef]
37. Wu, M.; Li, H.; Chen, W.; Wang, D.; He, Y.; Xu, L.; Ye, S.; Tan, G. A triplet stibinidene. *Chem* **2023**, *9*, 2573–2584. [CrossRef]
38. Schmid, P.; Bitschnau, B.; Finšgar, M.; Letofsky-Papst, I.; Rattenberger, J.; Saf, R.; Uhlig, F.; Torvisco, A. Characterization of Germanium Nanoparticles from Arylgermanium Trihydrides. *Chem. Eur. J.* **2024**, *30*, e202401382. [CrossRef] [PubMed]
39. Torvisco, A.; Uhlig, F.; Scheschkewitz, D. *Synthesis of Group 14 Metal-Containing Polymers*; Wiley-VCH Verlag GmbH & Co. KGaA: Hoboken, NJ, USA, 2019; pp. 61–84. [CrossRef]
40. Pugh, T.; Chilton, N.F.; Layfield, R.A. Antimony-ligated dysprosium single-molecule magnets as catalysts for stibine dehydrocoupling. *Chem. Sci.* **2017**, *8*, 2073–2080. [CrossRef] [PubMed]
41. Balázs, G.; Breunig, H.J.; Lork, E.; Offermann, W. Two Stable Hydrides of Antimony: RSbH2 and R(H)Sb−Sb(H)R (R = (Me3Si)2CH). *Organometallics* **2001**, *20*, 2666–2668. [CrossRef]
42. Ateş, M.; Breunig, H.J.; Güleç, S.; Offermann, W.; Häberle, K.; Dräger, M. Synthesen und Strukturen von Ethyl-, Propyl-, Butyl-und Mesitylantimon. *Chem. Ber.* **1989**, *122*, 473–478. [CrossRef]
43. Breunig, H.J.; Ebert, K.H.; Guelec, S.; Probst, J. Syntheses, structures, and equilibria of *o*-, *m*-, *p*-tolyl- and phenylantimony rings. *Chem. Ber.* **1995**, *128*, 599–603. [CrossRef]
44. Challenger, F.; Pritchard, F.; Jinks, J.R.A. Action of inorganic halides on organo-metallic compounds. *J. Chem. Soc. Trans.* **1924**, *125*, 864–875. [CrossRef]
45. Sobolev, A.N.; Romm, I.P.; Belsky, V.K.; Syutkina, O.P.; Guryanova, E.N. Structure analysis of triaryl derivatives of the group V elements III. Molecular Structure and Spectra of Tris(2,6-Dimethylphenyl)Stibine, $C_{24}H_{27}Sb$. *J. Organomet. Chem.* **1981**, *209*, 49–55. [CrossRef]
46. Forster, G.E.; Begley, M.J.; Sowerby, D.B. Preparation and crystal structures of diphenylantimony(III) thiocyanate and bis(2,6-dimethylphenyl)antimony(III) thiocyanate. *J. Chem. Soc. Dalton Trans.* **1995**, *3*, 377–382. [CrossRef]
47. Breunig, H.J.; Kanig, W.; Soltani-Neshan, A. Bis- and tris(trimethylsilyl)methyl derivatives of antimony. *Polyhedron* **1983**, *2*, 291–292. [CrossRef]
48. Binder, J.; Fischer, R.C.; Flock, M.; Torvisco, A.; Uhlig, F. Novel Aryl Substituted Silanes Part I: Synthesis and Characterization of Diaryl Silicon Dichlorides. *Phosphorus, Sulfur Silicon Relat. Elem.* **2015**, *190*, 1980–1993. [CrossRef]
49. Millington, P.L.; Sowerby, D.B. Preparation and crystal structures of five organoantimony halides; (p-tolyl)antimony(III) dichloride and dibromide, diphenylantimony(III) bromide, (biphenyl-2,2′-diyl)antimony(III) chloride and bis(2′-chlorobiphenyl-2-yl)antimony(V) trichloride. *J. Organomet. Chem.* **1994**, *480*, 227–234. [CrossRef]
50. Meyer, E.A.; Castellano, R.K.; Diederich, F. Interactions with aromatic rings in chemical and biological recognition. *Angew. Chem. Int. Ed.* **2003**, *42*, 1210–1250. [CrossRef]
51. Nayak, S.K.; Sathishkumar, R.; Row, T.N.G. Directing role of functional groups in selective generation of C-H···p interactions: In situ cryo-crystallographic studies on benzyl derivatives. *CrystEngComm* **2010**, *12*, 3112–3118. [CrossRef]
52. Janiak, C. A critical account on p-p stacking in metal complexes with aromatic nitrogen-containing ligands. *J. Chem. Soc. Dalton Trans.* **2000**, *21*, 3885–3896. [CrossRef]
53. Hunter, C.A.; Sanders, J.K.M. The nature of p-p interactions. *J. Am. Chem. Soc.* **1990**, *112*, 5525–5534. [CrossRef]
54. Yao, Z.-F.; Wang, J.-Y.; Pei, J. Control of π–π Stacking via Crystal Engineering in Organic Conjugated Small Molecule Crystals. *Cryst. Growth Des.* **2018**, *18*, 7–15. [CrossRef]
55. Aakeroy, C.B.; Evans, T.A.; Seddon, K.R.; Palinko, I. The C-H···Cl hydrogen bond: Does it exist? *New J. Chem.* **1999**, *23*, 145–152. [CrossRef]
56. Balamurugan, V.; Hundal, M.S.; Mukherjee, R. First Systematic Investigation of C-H···Cl Hydrogen Bonding Using Inorganic Supramolecular Synthons: Lamellar, Stitched Stair-Case, Linked-Ladder, and Helical Structures. *Chem. Eur. J.* **2004**, *10*, 1683–1690. [CrossRef] [PubMed]

57. Balamurugan, V.; Jacob, W.; Mukherjee, J.; Mukherjee, R. Designing neutral coordination networks using inorganic supramolecular synthons: Combination of coordination chemistry and C–H···Cl hydrogen bonding. *CrystEngComm* **2004**, *6*, 396–400. [CrossRef]
58. Nangia, A. Database research in crystal engineering. *CrystEngComm* **2002**, *4*, 93–101. [CrossRef]
59. Nelyubina, Y.V.; Antipin, M.Y.; Lyssenko, K.A. Are Halide···Halide Contacts a Feature of Rock-Salts Only? *J. Phys. Chem. A* **2007**, *111*, 1091–1095. [CrossRef]
60. Willett, R.D.; Twamley, B.; Montfrooij, W.; Granroth, G.E.; Nagler, S.E.; Hall, D.W.; Park, J.-H.; Watson, B.C.; Meisel, M.W.; Talham, D.R. Dimethylammonium Trichlorocuprate(II): Structural Transition, Low-Temperature Crystal Structure, and Unusual Two-Magnetic Chain Structure Dictated by Nonbonding Chloride−Chloride Contacts. *Inorg. Chem.* **2006**, *45*, 7689–7697. [CrossRef] [PubMed]
61. Caracelli, I.; Haiduc, I.; Zukerman-Schpector, J.; Tiekink, E.R.T. Delocalised antimony(lone pair)-and bismuth-(lone pair)...π(arene) interactions: Supramolecular assembly and other considerations. *Coord. Chem. Rev.* **2013**, *257*, 2863–2879. [CrossRef]
62. Mundt, O.; Becker, G.; Stadelmann, H.; Thurn, H. Element—Element-Bindungen. VII. Intermolekulare Wechselwirkungen bei Dihalogen(phenyl)stibanen. *Z. Anorg. Allg. Chem.* **1992**, *617*, 59–71. [CrossRef]
63. Wetzel, J. Crystal-structure investigation of the triphenyls of Bi, As and Sb. *Z. Kristallogr. Kristallgeom. Kristallphys. Kristallchem.* **1942**, *104*, 305–347.
64. Adams, E.A.; Kolis, J.W.; Pennington, W.T. Structure of triphenylstibine. *Acta Crystallogr. Sect. C Cryst. Struct. Commun.* **1990**, *46*, 917–919. [CrossRef]
65. Sharutin, V.V.; Sharutina, O.K.; Kazakov, M.V. Tri-*m*-tolylantimony dibenzoate: Synthesis and structure. *Russ. J. Inorg. Chem.* **2014**, *59*, 1115–1118. [CrossRef]
66. Sharutin, N.S.V.; CSD Communication. Private communication, 2016.
67. García-Monforte, M.Á.; Baya, M.; Joven-Sancho, D.; Ara, I.; Martín, A.; Menjón, B. Increasing Lewis acidity in perchlorophenyl derivatives of antimony. *J. Organomet. Chem.* **2019**, *897*, 185–191. [CrossRef]
68. Efremov, A.N.; Sharutin, V.V. Triphenylantimony and Pentaphenylantimony as the Starting Compounds for the Synthesis of Antimony(V) Phenyl Derivatives. Structure of Triphenylantimony, Bis(3,4-difluorobenzoato)triphenylantimony and Tetraphenylantimony Carbonate. *Russ. J. Coord. Chem.* **2023**, *49*, 56–62. [CrossRef]
69. Effendy; Grigsby, W.J.; Hart, R.D.; Raston, C.L.; Skelton, B.W.; White, A.H. Structural Characterization of Some Novel Oxidation Products of Triphenylstibine. *Aust. J. Chem.* **1997**, *50*, 675–682. [CrossRef]
70. Sobolev, A.N.; Romm, I.P.; Belsky, V.K.; Guryanova, E.N. Structure analysis of triaryl derivatives of the group V elements. crystal and molecular structure of tri-p-tolylantimony, $C_{21}H_{21}Sb$. *J. Organomet. Chem.* **1979**, *179*, 153–157. [CrossRef]
71. Sharma, P.; Cabrera, A.; Rosas, N.; Le Lagadec, R.; Hernandez, S.; Valdes, J.; Arias, J.L.; Ambrouse, C.V. Crystal structures of tri(*o*-tolyl)stibine in two crystal forms. *Main Group Met. Chem.* **1998**, *21*, 303–308. [CrossRef]
72. Lee, E.J.; Hong, J.S.; Kim, T.-J.; Kang, Y.; Han, E.M.; Lee, J.J.; Song, K.; Kim, D.-U. Synthesis and structural characterization of main group 15 organometallics R_3M and $R(Ph)_2P$(:N-Ar) (M = P, Sb, Bi; R = phenanthrenyl; Ar = 2,6-^{i}Pr$_2$-C_6H_3). *Bull. Korean Chem. Soc.* **2005**, *26*, 1946–1952. [CrossRef]
73. Ates, M.; Breunig, H.J.; Ebert, K.H.; Kaller, R.; Draeger, M.; Behrens, U. Structures of tetramesityldistibine and trimesitylstibine. *Z. Naturforsch. B Chem. Sci.* **1992**, *47*, 503–508. [CrossRef]
74. Sasaki, S.; Sutoh, K.; Murakami, F.; Yoshifuji, M. Synthesis, Structure, and Redox Properties of the Extremely Crowded Triarylpnictogens: Tris(2,4,6-triisopropylphenyl)phosphine, Arsine, Stibine, and Bismuthine. *J. Am. Chem. Soc.* **2002**, *124*, 14830–14831. [CrossRef]
75. Lindquist-Kleissler, B.; Johnstone, T.C. Models of the putative antimony(v)–diolate motifs in antileishmanial pentavalent antimonial drugs. *Dalton Trans.* **2023**, *52*, 9229–9237. [CrossRef]
76. Wenger, J.S.; Weng, M.; George, G.N.; Johnstone, T.C. Isolation, bonding and reactivity of a monomeric stibine oxide. *Nat. Chem.* **2023**, *15*, 633–640. [CrossRef]
77. Fritzsche, A.-M.; Scholz, S.; Krasowska, M.; Bhattacharyya, K.; Toma, A.M.; Silvestru, C.; Korb, M.; Rüffer, T.; Lang, H.; Auer, A.A.; et al. Evaluation of bismuth-based dispersion energy donors–synthesis, structure and theoretical study of 2-biphenylbismuth(iii) derivatives. *Phys. Chem. Chem. Phys.* **2020**, *22*, 10189–10211. [CrossRef]
78. Alvarez, S. A cartography of the van der Waals territories. *Dalton Trans.* **2013**, *42*, 8617–8636. [CrossRef] [PubMed]
79. Allen, F.H. The Cambridge Structural Database: A quarter of a million crystal structures and rising. *Acta Crystallogr. Sect. B* **2002**, *58*, 380–388. [CrossRef] [PubMed]
80. Shawkataly, O.B.; Hussien Abdelnasir, H.M.; Rosli, M.M. Crystal structure of bromidobis(naphthalen-1-yl)antimony(III). *Acta Crystallogr. Sect. E.* **2014**, *70*, m351. [CrossRef] [PubMed]
81. Rheingold, A.L.; CSD Communication. Private communication, 2019.
82. Becker, G.; Mundt, O.; Sachs, M.; Breunig, H.J.; Lork, E.; Probst, J.; Silvestru, A. Untersuchungen am Chlordiphenyl-und Tribenzylstiban sowie am Tribenzyldibromstiboran–Molekülstrukturen und Isotypie. *Z. Anorg. Allg. Chem.* **2001**, *627*, 699–714. [CrossRef]
83. Beckmann, J.; Heek, T.; Takahashi, M. The First Mixed-Valent Antimony(III/V) Oxo Clusters (2,6-$Mes_2C_6H_3Sb)_2(ClSb)_4O_8$ and (2,6-$Mes_2C_6H_3Sb)_4(ClSb)_4(HOSb)_2O_{14}$. *Organometallics* **2007**, *26*, 3633–3635. [CrossRef]

84. Twamley, B.; Sofield, C.D.; Olmstead, M.M.; Power, P.P. Homologous Series of Heavier Element Dipnictenes 2,6-$Ar_2H_3C_6E{=}EC_6H_3$-2,6-Ar_2 (E = P, As, Sb, Bi; Ar = Mes = C_6H_2-2,4,6-Me_3; or Trip = C_6H_2-2,4,6-$^iPr_3$) Stabilized by *m*-Terphenyl Ligands. *J. Am. Chem. Soc.* **1999**, *121*, 3357–3367. [CrossRef]
85. Nag, E.; Kulkarni, A.; Gorantla, S.M.N.V.T.; Graw, N.; Francis, M.; Herbst-Irmer, R.; Stalke, D.; Roesky, H.W.; Mondal, K.C.; Roy, S. Fluorescent organo-antimony compounds as precursors for syntheses of redox-active trimeric and dimeric alkali metal antimonides: An insight into electron transfer reduction processes. *Dalton Trans.* **2022**, *51*, 1791–1805. [CrossRef]
86. Cowley, A.H.; Nunn, C.M.; Westmoreland, D.L. Structure of tetramesityldistibane. *Acta Crystallogr. Sect. C: Cryst. Struct. Commun.* **1990**, *46*, 774–776. [CrossRef]
87. Deuten, K.V.; Rehder, D. Tetraphenyldistibine, $C_{24}H_{20}Sb_2$. *Cryst. Struct. Commun.* **1980**, *9*, 167–171.
88. Becker, G.; Freudenblum, H.; Witthauer, C. Trimethylsilylverbindungen der Vb-Elemente. VI. Synthese, Molekül-und Kristallstruktur des Tetrakis(trimethylsilyl)distibans im Vergleich mit Tetraphenyldistiban. *Z. Anorg. Allg. Chem.* **1982**, *492*, 37–51. [CrossRef]
89. Bruker. *APEX2 and SAINT*; Bruker AXS Inc.: Madison, WI, USA, 2012.
90. Blessing, R.H. An empirical correction for absorption anisotropy. *Acta Crystallogr. Sect. A Found. Adv.* **1995**, *51*, 33–38. [CrossRef] [PubMed]
91. Sheldrick, G.M. *SADABS, Version 2.10, Siemens Area Detector Correction*; Georg-August-Universität: Göttingen, Germany, 2003.
92. Bruker. *TWINABS*; Bruker AXS Inc.: Madison, WI, USA, 2001.
93. Sheldrick, G.M. SHELXT-Integrated space-group and crystal-structure determination. *Acta Crystallogr. Sect. A Found. Adv.* **2015**, *71*, 3–8. [CrossRef] [PubMed]
94. Sheldrick, G.M. Phase annealing in SHELX-90: Direct methods for larger structures. *Acta Crystallogr. Sect. A Found. Adv.* **1990**, *46*, 467–473. [CrossRef]
95. Sheldrick, G.M. *SHELXS97*; University of Göttingen: Göttingen, Germany, 1997.
96. Sheldrick, G.M. A short history of SHELX. *Acta Crystallogr. Sect. A Found. Adv.* **2008**, *64*, 112–122. [CrossRef] [PubMed]
97. Sheldrick, G.M. Crystal structure refinement with SHELXL. *Acta Crystallogr. Sect. C Struct. Chem.* **2015**, *71*, 3–8. [CrossRef] [PubMed]
98. Huebschle, C.B.; Sheldrick, G.M.; Dittrich, B. ShelXle: A Qt graphical user interface for SHELXL. *J. Appl. Crystallogr.* **2011**, *44*, 1281–1284. [CrossRef]
99. Spek, A.L. Single-crystal structure validation with the program PLATON. *J. Appl. Crystallogr.* **2003**, *36*, 7–13. [CrossRef]
100. Spek, A.L. Structure validation in chemical crystallography. *Acta Crystallogr. Sect. D.* **2009**, *65*, 148–155. [CrossRef]
101. Müller, P.; Herbst-Irmer, R.; Spek, A.L.; Schneider, T.R.; Sawaya, M.R. *Crystal Structure Refinement: A Crystallographer's Guide to SHELXL*; Oxford University Press: Oxford, UK, 2006; p. 232.
102. Macrae, C.F.; Bruno, I.J.; Chisholm, J.A.; Edgington, P.R.; McCabe, P.; Pidcock, E.; Rodriguez-Monge, L.; Taylor, R.; van de Streek, J.; Wood, P.A. Mercury CSD 2.0-new features for the visualization and investigation of crystal structures. *J. Appl. Crystallogr.* **2008**, *41*, 466–470. [CrossRef]
103. Putz, H.; Brandenburg, K. *Diamond-Crystal and Molecular Structure Visualization, 4.6.5*; Crystal Impact: Bonn, Germany, 2023.